Robotica (2015) volume 33, pp. 1609–1627. © Cambridge University Press 2014
doi:10.1017/S0263574714000940

Active global localization based on localizability for mobile robots

Yong Wang†,‡, Weidong Chen†,‡*, Jingchuan Wang†,‡ and Hesheng Wang†,‡

†*Department of Automation, Shanghai Jiao Tong University, and Key Laboratory of System Control and Information Processing, Ministry of Education of China, Shanghai 200240, China*
‡*State Key Laboratory of Robotics and System (HIT), Harbin 150001, China*

(Accepted March 17, 2014. First published online: April 25, 2014)

SUMMARY
In global localization under the framework of a particle filter, the acquiring of effective observations of the whole particle system will be greatly effected by the uncertainty of a prior-map, such as unspecific structures and noises. In this study, taking the uncertainty of the prior-map into account, a localizability-based action selection mechanism for mobile robots is proposed to accelerate the convergence of global localization. Localizability is defined to evaluate the observations according to the prior-map (probabilistic grid map) and observation (laser range-finder) models based on the Cramér-Rao Bound. The evaluation considers the uncertainty of the prior-map and does not need to extract any specific observation features. Essentially, localizability is the determinant of the inverse covariance matrix for localization. Specifically, at the beginning of every filtering step, the action, which makes the whole particle system to achieve the maximum localizability distinctness, is selected as the actual action. Then there will be the increased opportunities for accelerating the convergence of the particles, especially in the face of the prior-map with uncertainty. Additionally, the computational complexity of the proposed algorithm does not increase significantly, as the localizability is pre-cached off-line. In simulations, the proposed active algorithm is compared with the passive algorithm (i.e. global localization with the random robot actions) in environments with different degrees of uncertainty. In experiments, the effectiveness of the localizability is verified and then the comparative experiments are conducted based on an intelligent wheelchair platform in a real environment. Finally, the experimental results are compared and analyzed among the existing active algorithms. The results demonstrate that the proposed algorithm could accelerate the convergence of global localization and enhance the robustness against the system ambiguities, thereby reducing the failure probability of the convergence.

KEYWORDS: Active global localization; Quality of map; Localizability; Action selection for mobile robots; Particle filter.

1. Introduction

Localization is one of the key technologies in robotics. It plays a pivotal role for mobile robots in carrying out various tasks.[1] Localization problems are generally classified into the following categories. One is called "pose tracking:" the initial robot pose (position and heading) is known exactly or given, and the tracking of pose is maintained during the given mission.[2,3] The other one is called "global localization:" robot pose is determined in the absence of the initial one.[4–8] The aim of global localization is to reduce the ambiguities of the robot pose and localize itself with all possible haste according to the prior-map and the sensor data. But the random actions of mobile robots, especially in the face of much uncertainty of the prior-map, are often incapable of determining the

* Corresponding author. E-mail: wdchen@sjtu.edu.cn

https://doi.org/10.1017/S0263574714000940 Published online by Cambridge University Press

pose of a robot, or very inefficient. The challenging problem in global localization is still "where to move" or "where to look" so as to efficiently localize itself.

In some global localization research, a prior-map is usually a geometric map, which consists of geometric elements (point, line, or angle), or even a more minimalist map.[9–12] But in practice, a geometric map seems not to be accurate to evaluate the observations, especially when required to reflect unspecific structures and map noises. Thus, some authors have divided geometric map into several occupied cells or grids.[13–15] This contributes to evaluating the observations to a certain extent in consideration of the uncertainty of the prior-map, but the prior-map is still essentially geometric. With the development of mapping technologies, probabilistic grid maps (PGM) are applied in global localization more and more.[16] PGM allows an intuitive and convenient representation of the ambiguous information. It is generally used for representation of a real environment. Thus, some authors have begun to deal with global localization based on PGM, which can better approximate the models of the real environment and noisy sensors.[17] Furthermore, some extra information is added on PGM when solving the global localization problem.[18–20] For these algorithms, PGM is only utilized to represent the uncertainty, but not applied in guiding the robot actions. The random robot actions still lead to an inefficient convergence of the algorithms. In other words, this kind of global localization algorithms is passive.

To accelerate the convergence of global localization or enhance the robustness against the system ambiguities for reducing the probability of failed convergence, guiding robot actions to achieve the effective observations has become the main research trend, which is called active global localization. As the observations of actual robots are local, many active global localization algorithms naturally focus on increasing the effective observations of the whole system according to the prior-map, but not the actual robot's. To achieve the effective observations of the whole system, evaluation of observations based on the prior-map has become the key point. This determines that the prior-map has great effects on the convergence of global localization.[21] In general, observations in one pose can be evaluated according to the prior-map and observation models. But it is not so easy, because in many cases specific observation features are difficult to extract, especially when there is uncertainty on the prior-map, such as unspecific structures or noises. In the previous study,[22] based on the PGM, the authors controlled the robot to move to the place with the smaller entropy in order to improve the global localization efficiency. Entropy can evaluate observations considering uncertainty of the prior-map, but the entropy-based action selection mechanism will increase the computational load rapidly while the map area expands. The computational load will be extraordinarily high in a large-scale environment, and the entropy only evaluates the overall observation uncertainty without directional information. Later, some researchers used a particle filter (PF)[23] to improve the computational efficiency of the entropy-based action selection mechanism,[24] but the calculation is still complex in a large environment. In some recent active global localization research,[25,26] the hypothesis of the robot pose is reduced based on the geometric features. The algorithms used the geometric prior-map and needed to extract the specific observation features, which cannot deal with the unspecific structures or noises of the prior-map, limiting further applications.

The effective observations of the whole system can be found based on the prior-map and observation models. No matter what is considered, covariance of the possible poses (estimated through the observations) is a straight-forward solution for evaluation of the observations.[27] Censi adopted the Cramér-Rao Bound (CRB) to evaluate the observations.[28] The CRB gives the lower bound of the attainable covariance for localization. In fact, the covariance lower bound is related with the inverse of Fisher's Information Matrix (FIM), which reflects the observation information. The effectiveness of evaluating the observations through CRB has been analyzed and verified.[29,30] However, in the research, the analytic map model limits the implementation and real application.

In our previous work, a localizability matrix is defined to evaluate the observations of a robot in one pose.[31–33] It is calculated according to the prior-map and laser range-finder (LRF) observation models based on CRB. Different from ref. [28], the prior-map adopts PGM instead of the analytic map, whose discrete and statistical attributes make the evaluation of the observations convenient. Essentially, the localizability matrix can evaluate the observations taking account of the uncertainty of the prior-map without extraction of any specific observation features. We have utilized it to solve the pose-tracking problem,[31,32] and also tried to solve the global localization problem preliminarily.[33]

In this study, under the PF framework, a localizability-based action selection mechanism for mobile robots is proposed to accelerate the convergence of global localization. Localizability is denoted as

https://doi.org/10.1017/S0263574714000940 Published online by Cambridge University Press

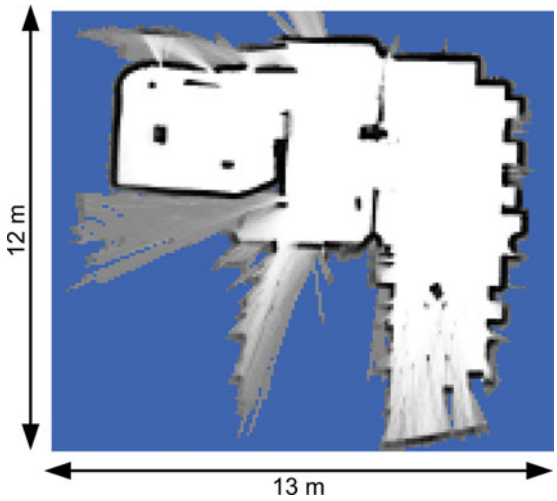


Fig. 1. Probabilistic grid map.

the determinant of the localizability matrix. Specifically, at the beginning of every filtering step, the action which makes the whole particle system to achieve the maximum localizability distinctness is selected as the actual action. Then the reason why the selected action could accelerate the convergence of the particles is analyzed. Additionally, the computational complexity of the proposed algorithm with the off-line pre-cache of localizability is given and also compared with the other active global localization algorithms. In simulations, the proposed active global localization algorithm is compared with the passive one (i.e. the global localization under PF framework with random robot actions) in environments with different degrees of uncertainty. In experiments, through precision comparison between covariance ellipses, which are estimated respectively by scan-matching algorithm[34] and localizability, the validation of localizability is analyzed. Then the comparative experiments between the passive and the proposed active algorithms are demonstrated in a real environment using an intelligent wheelchair. Finally, the experimental results are compared and analyzed with the existing active algorithms.

2. Estimation of Localizability

2.1. Prior-map and LRF observation models

The prior-map adopts the PGM as shown in Fig. 1, which can represent the uncertainty of environments more properly. It is constructed based on the incremental maximum likelihood method using the measurements of the odometer and LRF.[35] The gray and black areas stand for the obstacle and environment boundaries, where the occupied probability $\mu_{x,y}$ of the inner grid (x, y) is limited in $(0, 1]$. The white area means an accessible area, where $\mu_{x,y}$ is a 0 constant. The blue area denotes an inaccessible area, where $\mu_{x,y}$ is a -1 constant.

In this study, LRF is adopted as the exteroceptive sensor for observation. $\boldsymbol{p} = [x, y, \theta]$ is the robot pose. $r_{iE}(p, \varphi_i)$ denotes the expected measurement of the ith LRF ray. The total number of the LRF scanning rays is N_o, and then the function of LRF observation model can be defined as

$$r_i = r_{iE}(\boldsymbol{p}, \varphi_i) + \varepsilon_i, \quad i = 1, 2, \ldots, N_o, \tag{1}$$

where the term ε_i is assumed to be the Gaussian random variable with mean 0 and variance σ_i^2. In practice, it is difficult to construct the analytic function of the real environments. That means r_{iE} and ε_i including its variance σ_i^2 cannot be determined exactly. To solve this problem, a discrete and statistical LRF observation model is proposed to estimate r_{iE} and σ_i^2 as shown in Fig. 2.

In Fig. 2, the model relies on the discrete and statistical attributes of PGM, i.e. the distribution of gray and black grids, which reflect the LRF observation errors. The green line $\hat{r}_{iE}$ stands for the

https://doi.org/10.1017/S0263574714000940 Published online by Cambridge University Press

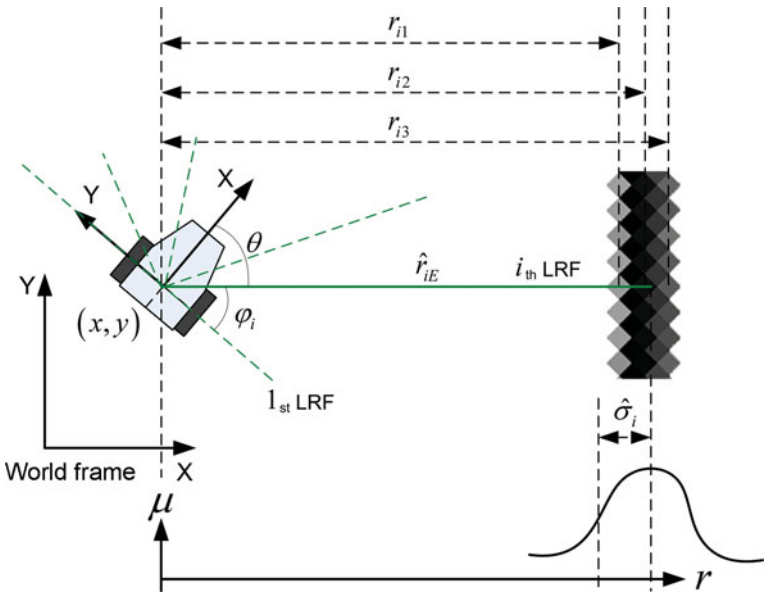


Fig. 2. A discrete and statistical LRF observation model based on PGM. The gray and black area is the enlarged partial drawing of the obstacle boundary on PGM.

estimated value of the expected measurement scanned by the *i*th LRF ray. It is defined as

$$\hat{r}_{iE} = \frac{\sum_j r_{ij}\mu_{ij}}{\sum_j \mu_{ij}}, \tag{2}$$

where r_{ij} is the measurement from robot to the *j*th grid of the obstacle boundary thickness, along the *i*th LRF ray direction, and μ_{ij} is the probability of the corresponding grid. Then the estimated variance $\hat{\sigma}_i^2$ is

$$\hat{\sigma}_i^2 = E_z(|r_{ij} - \hat{r}_{iE}|^2), \tag{3}$$

where E_z is the expection operator.

2.2. *Localizability matrix*

Taking account of the function of LRF observation model (1) and independence of each measurement of LRF ray, the probability density function $d(\boldsymbol{p}, z)$ of localization in pose $\boldsymbol{p}$ can be defined as

$$d(\boldsymbol{p}, z) = \prod_{i=1}^{n} d_i(r_i, map), \tag{4}$$

where r_i is the measurement of the *i*th LRF ray and z denotes the observations with Gaussian random noise.

Based on $d(\boldsymbol{p}, z)$, a series of possible poses of a robot can be estimated. The distribution of the possible poses reflects the localization uncertainty. In other words, the covariance of these possible poses can be utilized to estimate the localizability of the robot in the current pose. Through the CRB,[36] for any unbiased estimated pose $\hat{\boldsymbol{p}}$,

$$cov(\hat{\boldsymbol{p}}) \geq [\Im(p)]^{-1}, \tag{5}$$

where $\boldsymbol{cov}(\hat{\boldsymbol{p}})$ is the localization covariance for localization and $\Im(\boldsymbol{p})$ is the FIM. The inequality sign means that $\boldsymbol{cov}(\hat{p}) - [\Im(\boldsymbol{p})]^{-1}$ is a non-negative-definite matrix. Equation (5) indicates the lower bound of the localization covariance.

https://doi.org/10.1017/S0263574714000940 Published online by Cambridge University Press

The FIM $\Im(\boldsymbol{p})$ can be defined as[37]

$$\Im(\boldsymbol{p}) = E_z\left\{\frac{\partial \log d(\boldsymbol{p},\boldsymbol{z})}{\partial \boldsymbol{p}}^{\mathrm{T}}\frac{\partial \log d(\boldsymbol{p},\boldsymbol{z})}{\partial \boldsymbol{p}}\right\} = \sum_{i=1}^{N_o}\frac{1}{\sigma_i^2}\left[\frac{\partial r_{iE}}{\partial \boldsymbol{p}}^{\mathrm{T}}\frac{\partial r_{iE}}{\partial \boldsymbol{p}}\right]. \tag{6}$$

But as analyzed in Section 2.1, it is difficult to construct the analytic function of a real environment since r_{iE} and σ_i^2 cannot be calculated exactly. Thus, Eq. (6) needs to be discretized based on the discrete and statistical LRF observation model. First, using $\frac{\Delta \hat{r}_{iE}}{\Delta p} = [\ \frac{\Delta \hat{r}_{iE}}{\Delta x}\ \ \frac{\Delta \hat{r}_{iE}}{\Delta y}\ \ \frac{\Delta \hat{r}_{iE}}{\Delta \theta}\ ]$ to replace $\frac{\partial r_{iE}}{\partial p}$. Then substituting Eqs. (2) and (3) into Eq. (6), a discrete FIM can be obtained as

$$\hat{\Im}(\boldsymbol{p}) = \sum_{i=1}^{N_o}\frac{1}{\hat{\sigma}_i^2}\left[\frac{\Delta \hat{r}_{iE}}{\Delta \boldsymbol{p}}^{\mathrm{T}}\frac{\Delta \hat{r}_{iE}}{\Delta \boldsymbol{p}}\right] = \sum_{i=1}^{N_o}\frac{1}{\hat{\sigma}_i^2}\begin{bmatrix} \frac{\Delta \hat{r}_{iE}^2}{\Delta x^2} & \frac{\Delta \hat{r}_{iE}^2}{\Delta x \Delta y} & \frac{\Delta \hat{r}_{iE}^2}{\Delta x \Delta \theta} \\ \frac{\Delta \hat{r}_{iE}^2}{\Delta x \Delta y} & \frac{\Delta \hat{r}_{iE}^2}{\Delta y^2} & \frac{\Delta \hat{r}_{iE}^2}{\Delta y \Delta \theta} \\ \frac{\Delta \hat{r}_{iE}^2}{\Delta x \Delta \theta} & \frac{\Delta \hat{r}_{iE}^2}{\Delta y \Delta \theta} & \frac{\Delta \hat{r}_{iE}^2}{\Delta \theta^2} \end{bmatrix}, \tag{7}$$

where when $\Delta \boldsymbol{p}$ is small enough, the approximation is valid.

Equation (7) is defined as the localizability matrix. Different from the entropy, besides the uncertainty of the prior-map, the localizability matrix can represent both the respective and the coupling influences on localization among x, y, and θ states (i.e. directional information), which is adaptable to evaluate the observations in environments with different degrees of uncertainty.

2.3. Localizability

The covariance ellipse is able to represent the covariance intuitively,[38] which is usually utilized to evaluate the localization results. For example, the larger covariance ellipse means that the possible poses of a robot are distributed in a large area and the localization uncertainty is greater. From Eqs. (5)–(7), the expected covariance matrix for localization can be calculated as

$$\boldsymbol{cov}(\hat{\boldsymbol{p}}) = \left[\hat{\Im}(\boldsymbol{p})\right]^{-1} = \begin{bmatrix} q_{xx} & q_{xy} & q_{x\theta} \\ q_{yx} & q_{yy} & q_{y\theta} \\ q_{\theta x} & q_{\theta y} & q_{\theta\theta} \end{bmatrix}. \tag{8}$$

Taking $x - y$ covariance ellipse for example, the semi-major axis of ellipse is

$$E_{xy} = \sqrt{\frac{q_{xx}+q_{yy}}{2} + \sqrt{\frac{(q_{xx}^2 - q_{yy}^2)}{4} + q_{xy}^2}}. \tag{9}$$

The semi-minor axis of ellipse is

$$F_{xy} = \sqrt{\frac{q_{xx}+q_{yy}}{2} - \sqrt{\frac{(q_{xx}^2 - q_{yy}^2)}{4} + q_{xy}^2}}. \tag{10}$$

The directional angel of semi-major axis is

$$\tan(2\varphi_{xy}) = \frac{2q_{xy}}{q_{xx} - q_{yy}}, \tag{11}$$

where if $\tan\varphi_{xy}$ and q_{xy} are with the opposite signum, $\varphi_{xy} = \varphi_{xy} + \frac{\pi}{2}$. Let $\hat{\lambda}_x$ and $\hat{\lambda}_y$ be the eigenvalues of $\hat{\Im}_{xy}(\boldsymbol{p})$, then

$$E_{xy} \propto \hat{\lambda}_x^{-1},\ F_{xy} \propto \hat{\lambda}_y^{-1}. \tag{12}$$

https://doi.org/10.1017/S0263574714000940 Published online by Cambridge University Press

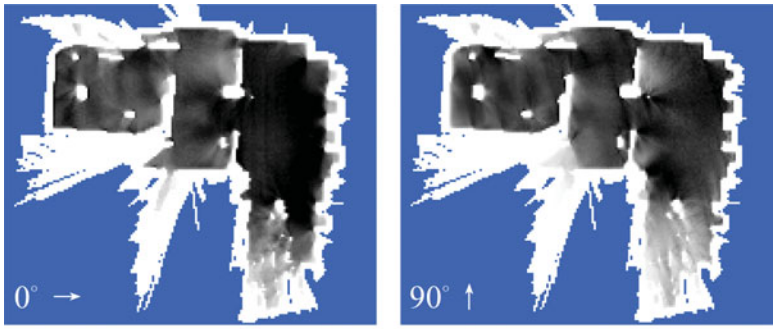


Fig. 3. Localizability estimation under the different observing directions.

As the area of the covariance ellipse is a measure of the global achievable accuracy,[28] and

$$\pi E_{xy} F_{xy} \propto \hat{\lambda}_x^{-1} \hat{\lambda}_y^{-1} \equiv \det\left(\hat{\mathfrak{F}}_{xy}(\boldsymbol{p})\right)^{-1}, \tag{13}$$

the determinant of $\hat{\mathfrak{F}}_{xy}(\boldsymbol{p})$ can reflect and weigh the achievable accuracy of localization. By analogy, the other covariance ellipses ($x-\theta$ and $y-\theta$ ones) can also be calculated through Eqs. (9)–(11). Then the determinant of the localizability matrix $\hat{\mathfrak{F}}(\boldsymbol{p})$ can be defined as the robot localizability in pose $\boldsymbol{p}$, as follows:

$$L(\boldsymbol{p}) = \det\left(\hat{\mathfrak{F}}(\boldsymbol{p})\right) \equiv \hat{\lambda}_x \hat{\lambda}_y \hat{\lambda}_\theta. \tag{14}$$

A larger $L(\boldsymbol{p})$ means that the mobile robots in this pose can achieve abundant possible observation information for localization. Figure 3 shows the localizability in every pose under the observing directions $\theta = 0^\circ$ and 90°. The darker color stands for the larger localizability.

3. Localizability-Based Active Global Localization

3.1. Basic framework

Taking account of the uncertainty of the prior-map, such as unspecific structures and map noises, localizability-based active global localization is proposed to accelerate the convergence of global localization. The algorithm is under the framework of classical PF[23] based on the PGM. The evaluation of the particle importance weight adopts the scan-matching algorithm.[34] The main improvement is the localizability-based action selection mechanism. Specifically, in every filtering step, all the possible robot actions are tested to see which one could generate the maximum localizability distinctness of the whole particle system. Then this action is selected as the actual one. The flowchart of the proposed algorithm is shown in Fig. 4.

As can be seen in Fig. 4, one filtering step of the proposed algorithm is composed of five processes (a–e). Through recursive execution, particles can eventually converge to the actual pose of the robot. Next, these processes are explained in detail.

3.1.1. Particle set initialization. In initialization, the particles $\boldsymbol{P}_{t=0} = \{\boldsymbol{p}_0^{(1)}, \boldsymbol{p}_0^{(2)}, \ldots, \boldsymbol{p}_0^{(N_p)}\}$ are distributed on the PGM with a uniform distribution as shown in Fig. 5. The yellow points denote all the N_p particles. The yellow circles represent the central circles of the convergence clusters, which are classified by the K-mean algorithm.[39] The purple circle denotes the pose of the simulated actual robot. The green circle is the robot pose estimated by the high-weighted particles. The red circle is the robot pose estimated by all the particles. Additionally, for convenience, the blue circle stands for one randomly chosen particle, which is used to explain the importance weight calculation.

3.1.2. Localizability-based action selection mechanism. The movement of a mobile robot is a partially observable Markov decision process. Its actions $\{A_i, i = 1, 2, \ldots, N_a\}$ can be generated according

https://doi.org/10.1017/S0263574714000940 Published online by Cambridge University Press

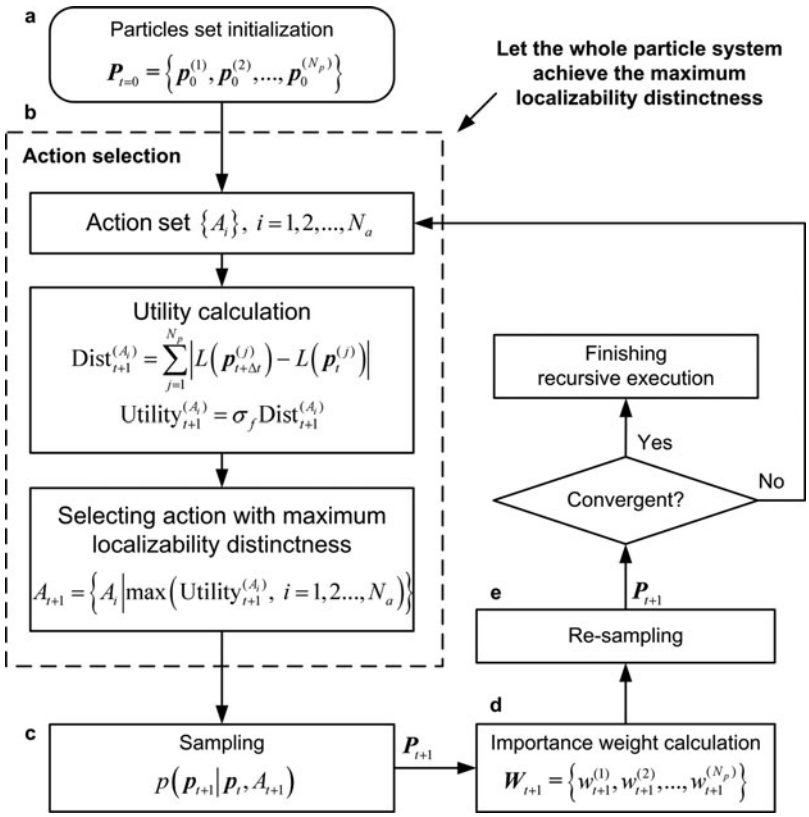


Fig. 4. The flowchart of the localizability-based active global localization.

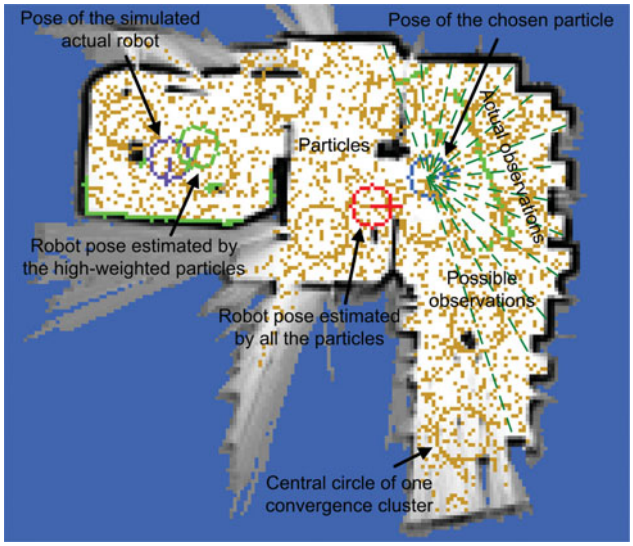


Fig. 5. The whole particle system with a uniform distribution.

to the collocation of the linear and angular velocity in one fixed executive time. All the actions are under the local frame of the robot. In order to ensure that the moving area of the mobile robot can cover its observing area, and also that the algorithm real-timing is acceptable, $N_a = 5$ is adopted.

https://doi.org/10.1017/S0263574714000940 Published online by Cambridge University Press

Specifically,

$$\begin{cases} A_1 = k_w \vec{w} & \leftarrow \text{Left turn} \\ A_2 = k_v \vec{v} + k_w \vec{w} & \nwarrow \text{Left and forward move} \\ A_3 = k_v \vec{v} & \uparrow \text{Forward move} \\ A_4 = k_v \vec{v} - k_w \vec{w} & \nearrow \text{Right and forward move} \\ A_5 = -k_w \vec{w} & \rightarrow \text{Right turn} \end{cases}, \tag{15}$$

where $\vec{v}$ is the linear velocity and $\vec{w}$ is the angular one. k_v and k_w are all the positive coefficients.

In the decision process, the action of every particle can be seen as the same as the action of the actual robot. After the supposed execution of one possible action A_i, the localizability distinctness among all the particles can be calculated as

$$\text{Dist}_{t+1}^{(A_i)} = \sum_{k=1}^{N_p} \left| L\left(p_{t+\Delta t}^{(k)}\right) - L\left(p_t^{(k)}\right) \right|, \tag{16}$$

where N_p is the particle number, Δt is the executive time of the action A_i, $p^{(k)}$ is the pose of the kth particle and L denotes the localizability. Essentially, $\text{Dist}_{t+1}^{(A_i)}$ reflects the trend of the possible observation distinctness after the execution of the action A_i.

Taking the influence from the dynamic obstacles into account, we designed an accessible factor σ_f for every action. Then the final utility of the action A_i can be determined as

$$\text{Utility}_{t+1}^{(A_i)} = \sigma_f \text{Dist}_{t+1}^{(A_i)}. \tag{17}$$

Specifically, when LRF detected the dynamic obstacles in the forward direction of action A_i, let $\sigma_f = 0$, or let $\sigma_f = 1$. Finally, the actual action is chosen according to Eq. (18):

$$A_{t+1} = \left\{ A_i \left| \max\left(\text{Utility}_{t+1}^{(A_i)}, i = 1, 2, \ldots, N_a = 5\right) \right. \right\}. \tag{18}$$

3.1.3. Sampling. Once the selected action is actually executed by the mobile robot, the sampling process continues. The new sampled particle set $\boldsymbol{P}_{t+1}^*$ is updated based on the Markov motion model $p\left(\boldsymbol{p}_{t+1} \middle| \boldsymbol{p}_t, A_{t+1}\right)$. In practice, it is usually sampled according to the calibrated odometer with a small amount of Gaussian noise.

3.1.4. Importance weight calculation. The particle importance weights $\boldsymbol{W}_{t+1} = \{w_{t+1}^{(1)}, w_{t+1}^{(2)}, \ldots, w_{t+1}^{(N_p)}\}$ are evaluated according to both the actual observations (from the LRF) and the possible ones (from the prior-map). For a particle (i.e. the blue circle in Fig. 5), the actual observations are represented by the N_o points (green), and the possible ones are represented by the N_o dashed rays (dark green). Based on the scan-matching algorithm,[34] the importance weight $w_{t+1}^{(k)}$ of the kth particle can be calculated as

$$w_{t+1}^{(k)} = \frac{1}{N_o} \sum_{k=1}^{N_o} \left\{ \mu\left(g(r_j^{(k)})\right) \left[\frac{\min\left(D_j^{(k)}, D_j^{(LRF)}\right)}{\max\left(D_j^{(k)}, D_j^{(LRF)}\right)} \right]^2 \right\}_{t+1} w_t^{(k)}, \tag{19}$$

where $w_t^{(k)}$ is the importance weight in the last t step; $\boldsymbol{g}(r_j^{(k)})$ is the endpoint of the jth LRF ray from the actual observations, where if $\mu = -1$, let $\mu = 0$ here; $D_j^{(k)}$ is the measurement of the jth LRF ray from the possible observations and $D_j^{(\text{LRF})}$ is the measurement of the jth ray from the actual observations. $w_{t+1}^{(k)}$ approaches to 1 stand for the similar observations and to 0 represent the distinctive ones.

https://doi.org/10.1017/S0263574714000940 Published online by Cambridge University Press

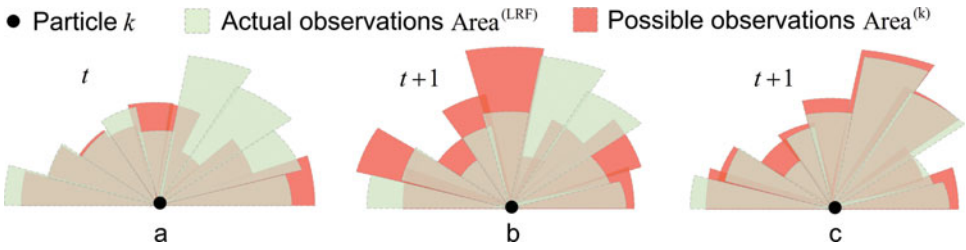


Fig. 6. Area ratio between the actual and possible observations.

3.1.5. Re-sampling. When necessary, the particles will be re-sampled based on the roulette method.[35] After the re-sampling process, the particle set $\boldsymbol{P}_{t+1}$ is updated and the importance weight $w_{t+1}^{(k)}$ of each particle is reset (in this process, the symbols do not change for conciseness). Finally, with the normalized importance weight $\tilde{w}_{t+1}^{(k)}$, the robot pose is estimated through Eq. (20):

$$\boldsymbol{p}_{t+1} = \sum_{k} \tilde{w}_{t+1}^{(k)} \boldsymbol{p}_{t+1}^{(k)}, \tag{20}$$

where k is the number of particles, which is variable because under different situations the robot pose can be estimated through only parts of particles that have high importance weight, or through all the particles.

3.2. Convergence analysis

The proposed active global localization is under the framework of PF. Both the sampling and re-sampling processes will bring randomicity information into the localization system in each filtering step. Since introducing the localizability-based action selection mechanism does not change the principle of PF, the convergence of the proposed algorithm will not be changed. Also, there is no Local Minimum problem in this algorithm. Next, the acceleration principle of convergence for the proposed algorithm will be analyzed.

The importance weight of a particle, i.e. Eq. (19), can be seen as the area ratio

$$w_{t+1}^{(k)} \in \frac{\text{Area}^{\cap}\left(\text{Area}_{t+1}^{(\text{LRF})}, \text{Area}_{t+1}^{(k)}\right)}{\text{Area}^{\cup}\left(\text{Area}_{t+1}^{(\text{LRF})}, \text{Area}_{t+1}^{(k)}\right)}, \tag{21}$$

where $\text{Area}^{\cap}$ means to calculate the overlapping area and $\text{Area}^{\cup}$ means to calculate the incorporative one. $\text{Area}_{t+1}^{(\text{LRF})}$ is the area of the actual observations from the LRF and $\text{Area}_{t+1}^{(k)}$ is the area of the possible observations from the prior-map in the kth particle pose. The area ratio in the t step is shown in Fig. 6(a).

The actual observations are local and in most situations would not change obviously during a small movement, while the sum of the possible observations from all the particles contains the global information and would change dramatically. The larger distinctness between $\text{Area}_{t}^{(k)}$ and $\text{Area}_{t+1}^{(k)}$ (for all the particles) will increase the opportunities that, the distinctness between $\text{Area}_{t+1}^{(\text{LRF})}$ and $\text{Area}_{t+1}^{(k)}$ also becomes larger, especially for the particles which depart from the actual pose of the robot. This situation is shown in Fig. 6(b). Fortunately, for the particles which are near the actual pose of the robot, the actual and possible observations will still match each other as can be seen in Fig. 6(c). This mechanism increases the opportunities that eliminate the particles with low importance weight quickly. Additionally, the maintained particles are of high reliability.

Because the localizability is defined to evaluate the observations of a robot in one pose, its distinctness essentially represents the distinctness of the possible observations. Thus, controlling the mobile robot to execute action A_{t+1}, which results in the maximum localizability distinctness of the whole particle system, can accelerate the convergence of global localization. Furthermore, experiments were done to verify the above analysis, as described in Section 4.

https://doi.org/10.1017/S0263574714000940 Published online by Cambridge University Press

Table I. Comparison of computational complexity of selecting one action.

Existing active algorithms	Practical computational complexity
ref. [26]	$O\left(N_h^d \times N_o^d \times N_a^d\right)$
ref. [25]	$O\left(N_h^2 \times N_o \times N_a\right)$
ref. [24]	$O\left(N_p^2 \cdot N_a\right)$
ref. [22]	$O\left(N_m \times N_g \times N_a\right)$
[Proposed]	$O\left(N_p \cdot N_a\right)$

3.3. Computational complexity

From the localizability matrix Eq. (7) and the functions of the action selection mechanism Eqs. (16)–(18), the theoretical computational complexity of selecting one action is $O(N_p \cdot (N_o \cdot 2N_s \cdot N_e) \cdot N_a)$, where N_p is the particle number, N_o is the LRF ray number, $N_s \equiv 3$ is the state space of p, $N_e \approx 4$ is the traversing thickness of the obstacle boundary, and N_a is the action number. But in practice, localizability in every pose can be calculated off-line based on the prior-map, so $O\left(N_o \cdot 2N_s \cdot N_e\right)$ becomes $O\left(1\right)$. Finally, the practical computational complexity of selecting one action changes to $O(N_p \cdot N_a)$, which does not increase the computational complexity significantly after introducing the action selection mechanism into the passive algorithm.

In Table I, the practical computational complexity of selecting one action is compared among the proposed and the existing active global localization algorithms.

In refs. [25] and [26], N_h is the number of pose hypotheses and d is the search depth of Bayesian network. Although the computational complexity is small, these algorithms used the geometric prior-map and much more time will be consumed in extraction of observation features. In ref. [22], N_m is the number of the possible pose states and N_g is the number of Gaussian distributions. As N_m increases remarkably with the environment size, the real-timing of the algorithm is a big problem. The algorithm in ref. [24] is improved compared to ref. [22]. Its computational complexity is smaller than ref. 22, but is still larger than the proposed algorithm.

4. Simulations and Experiments

4.1. Preliminaries

4.1.1. Hardware and software platforms. The hardware platform for simulations is a personal computer (Intel Core2 Duo E7200 2.5GHz CPU, DDR2–800 2G RAM). The hardware platform for experiments is an intelligent wheelchair named "JiaoLong" as shown in Fig. 7. Based on this platform, the algorithm is executed on an Industrial Computer (Intel Core Duo T2500 2.0G CPU, DDR2–667 3G RAM). The wheelchair adopts DC motors with two-wheeled differential driving controlled by a DSP (digital signal processor) motion controller. An encoder-based odometer[40] and a LRF (SICK LMS111) are included.

In simulations and experiments, the software platform is CARMEN toolkit in Linux SUSE.[41] During comparison of the different global localization algorithms, the code of passive algorithm, i.e. the classical PF algorithm with random robot actions,[23] comes directly from CARMEN itself; the code of the proposed active algorithm is realized through the add-on developments based on CARMEN. Before simulations and experiments, the global PGM is built first of all. Then the localizability in every pose is calculated and pre-cached off-line. Because the observing area of LRF is not panoramic (only $0 - 180^\circ$), the pre-cached localizability needs to be calculated under N_d different observing directions respectively. A particular direction partition could bring more accurate estimation of the observations, but the execution time (off-line) will become larger. In practice, the number of the observing directions is set as $N_d = 360$ with a resolution of 1°. The pre-cached localizability was previously shown in Fig. 3.

4.1.2. Reference standards. In simulation, the actual robot pose is known exactly, so the different convergence statuses of particles can be distinguished clearly. Then we classified the convergence statuses into three types based on the K-mean algorithm[39] and Mahalanobis distance,[42] which are

https://doi.org/10.1017/S0263574714000940 Published online by Cambridge University Press

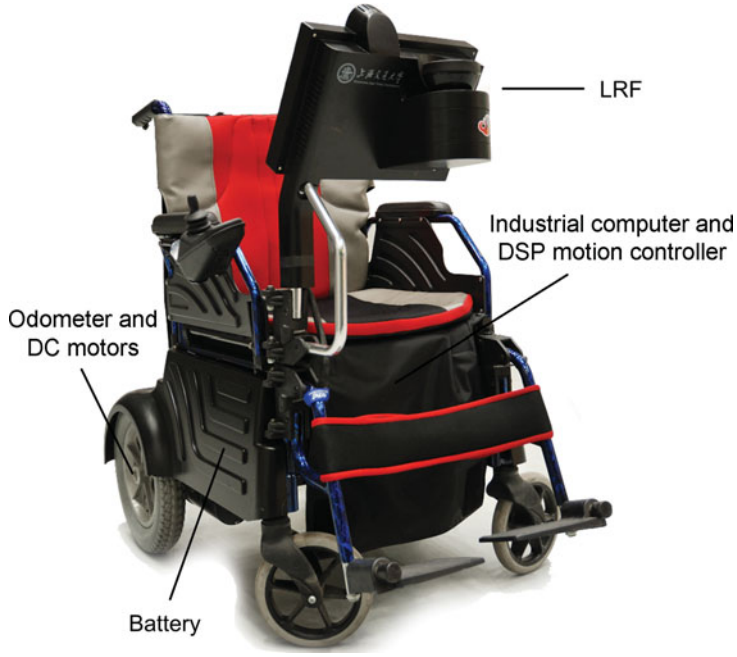


Fig. 7. "JiaoLong" intelligent wheelchair.

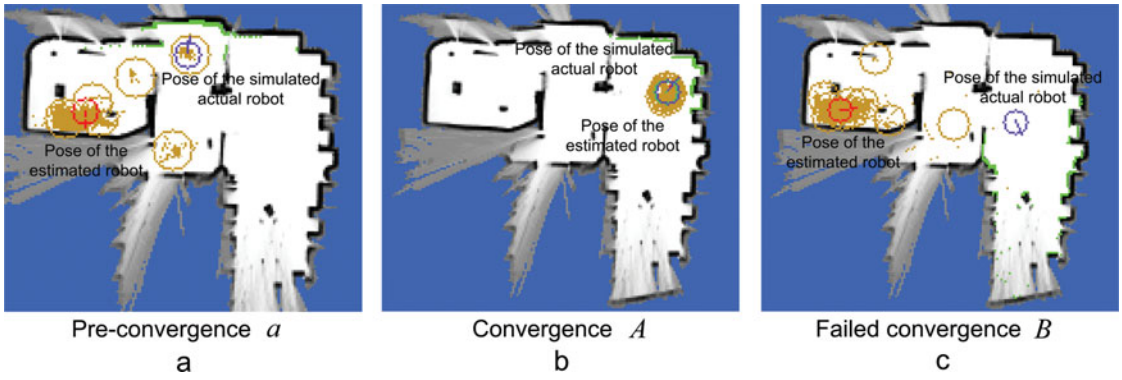


Fig. 8. Convergence status of particles a, A, and B.

shown in Fig. 8. Please note, here the actual robot pose is only used for analysis of convergence results.

In Fig. 8(a), the convergence status a means that the pre-convergence has completed and particles have been classified into several obvious convergence clusters. For the convergence status A in Fig. 8(b), most of the particles have converged into one cluster and the estimated pose approaches to the actual one. In Fig. 8(c), the convergence status B represents a failed convergence that, although most of particles have converged into one cluster, the estimated pose departs from the actual one. The judgment conditions of the different convergence statuses are shown in Table II.

In Table II, M_p is the Mahalanobis distance between the estimated robot pose and the central points of the convergence clusters, and M_r is the Mahalanobis distance between the actual robot pose and the central points of the convergence clusters. One grid stands for 0.1 m.

Additionally, all the parameters used in simulations and experiments are listed in Table III.

4.2. Simulations

In simulations, the passive and the proposed active global localization algorithms are compared in environments with different degrees of uncertainty as presented in Fig. 9. Compared to the other places, scenario T1 has a few unspecific structures and map noises. Generally, it has distinct observation features. Scenario T2 is an inner room. It has similar observation features overall, with more unspecific

https://doi.org/10.1017/S0263574714000940 Published online by Cambridge University Press

Table II. Judgment conditions of the different convergence statuses.

Convergence status	Judgment conditions
a	1. More than 80% particles are limited in 10 central circles of the convergence clusters 2. $M_p > 10$ grids or $M_r > 10$ grids
A	1. The same as judgment condition 1 of *a* 2. $M_p < 2$ grids and $M_r < 2$ grids
B	1. The same as judgment condition 1 of *a* 2. $M_p < 2$ grids and $M_r > 20$ grids

Table III. Algorithm parameters in simulations and experiments.

Description	Parameters
Map resolution (size of one grid)	0.1×0.1 m^2
Discrete step in Eq. (7)	$\Delta x = \Delta y = 0.1$ m, $\Delta\theta = 1^\circ$
Max-scanning distance of the LRF	$D_{\max} = 20$ m
Scanning area, resolution, and ray number of the LRF	$0 - 180^\circ$, 1°, $N_o = 181$
Odometer error	10% Gaussian error
LRF error and observation noise	0.5% Gaussian error, noise contained in map
Number of particles	$N_p = 3000$
Number and resolution of the observing direction for pre-cache	$N_d = 360$, 1°
Number of the actions	$N_a = 5$
Linear velocity of the action	$\vec{v} = 0.4$m/s
Linear velocity coefficient	$k_v = 1.0$
Angular velocity of the action	$\vec{w} = 20^\circ$/s
Angular velocity coefficient	$k_w = 1.0$
Executive time of the action	$\Delta t = 2.0$s
Lower threshold of the high importance weight $w_t^{(k)}$	0.7

structures and noises. Scenario T3 is a hallway. It has a few unspecific structures and noises, and in general very similar observation features, which will import the comparable ambiguities.

Because the observations from LRF are not panoramic, for every different scenario, we performed four groups of simulations, under "UP," "DOWN," "LEFT," and "RIGHT" initial observing directions. For every group, 20 comparative simulations were done. In each comparative simulation, the passive algorithm is compared with the proposed active algorithm once. During one comparison, the initial conditions, such as the initial actual robot pose (not known to the robot), the initial particle distribution and so on, are same. But for the sake of collecting the statistical results, the initial conditions are random for the different comparative simulations.

Generally, particles will converge to convergence status *a* at first. Then particles continue to converge to either status *A* or *B*. However, it is possible that particles converge to status *A* or *B* directly without an obvious transitional status *a*. As mentioned above, convergence status *A* means a normal convergence and *B* stands for a failed one. In simulations, we adopt the statistical approach to compare the results. As analyzed in Section 3.3, the execution time of the passive and the proposed active algorithms are nearly the same, so the convergence steps are used to represent the convergence efficiency of the algorithms. The average convergence steps in the different scenarios T1, T2, and T3 are compared in Table IV (for each scenario, 20×4 simulations are done). For convergence status *B*, what was recorded are the failed and total times of simulations.

From Table IV, no matter in which scenario, the average convergence steps to status *a* or *A* of the proposed active algorithm are smaller than the passive algorithm. Scenario T2, especially T3, will bring more ambiguities. The passive algorithm in these scenarios is easy to fail (49 failed times in the total 80 simulations in T3). The proposed active algorithm failed fewer times (28 times). The results show that, after taking the uncertainty of the prior-map into account, the proposed active algorithm could accelerate the convergence of the global localization effectively. Although the observation

https://doi.org/10.1017/S0263574714000940 Published online by Cambridge University Press

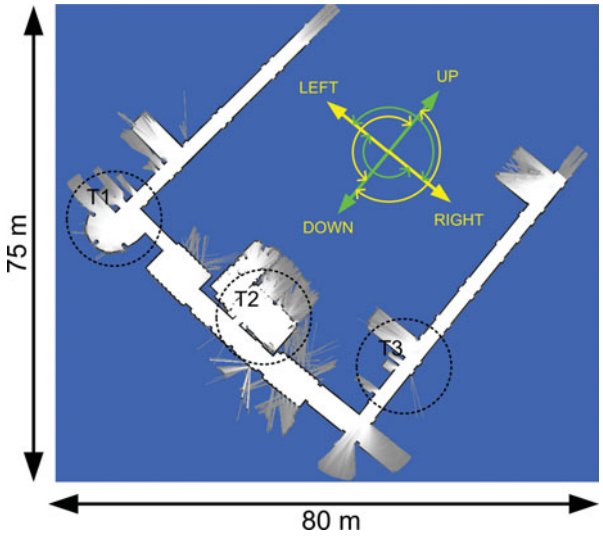


Fig. 9. Scenarios with different degrees of uncertainty.

Table IV. Comparison of the average convergence steps.

	Passive algorithm			Proposed active algorithm		
	Convergence status			Convergence status		
	a	*A*	*B*	*a*	*A*	*B*
T1	31.9 steps	123.6 steps	2/80	25.0 steps	85.9 steps	0/80
T2	42.8 steps	153.8 steps	15/80	36.1 steps	111.7 steps	6/80
T3	25.0 steps	234.2 steps	49/80	17.5 steps	186.9 steps	28/80

features are not extracted specifically in estimation of the localizability, the proposed algorithm still enhances the robustness of global localization in the environments with different degrees of uncertainty.

Figure 10 is a bar chart comparing the convergence steps to status *A*. In Figs. 10(a)–(c), the comparative results are chosen randomly from the comparative simulations for the different scenarios (except the failed ones). All the chosen results are compared in Fig. 10(d). It is indicated that, in different scenarios, the proposed active algorithm converges much more quickly than the passive one for most situations. The results clearly demonstrate the benefit of considering the uncertainty of the prior-map: it could accelerate the convergence of global localization.

4.3. Experiments

4.3.1. Validation of localizability. Covariance ellipse can reflect the covariance intuitively.[38] In this section, it is adopted to evaluate the effectiveness of localizability. First, the "JiaoLong" wheelchair is fixed in one pose. The classical PF algorithm[23] based on the scan-matching method (with re-sampling) is applied using the real-time LRF measurements. Until the estimated pose is steady, the particle distribution can be enclosed using an ellipse, i.e. the covariance ellipse (red real-line ellipse in Fig. 11). Second, the covariance and the corresponding ellipse in the same pose can be calculated directly according to the localizability matrix (see Section 2.3; green broken-line ellipse in Fig. 11). Finally, these two ellipses are compared and analyzed.

In Fig. 11(a), the covariance ellipses estimated by the classical PF algorithm and the localizability are small and consistent with each other. This is accurate, because the wheelchair observations have clear and specific structures. In Fig. 11(b), the two covariance ellipses are still consistent. Both the covariance ellipses show that the localization uncertainty along the y axis is larger than the one along the x axis. This expression is accurate. Because the wheelchair faces a wall, there is a little structure diversity of the observations along the y axis. In Fig. 11(c), the wheelchair faces a glass door

https://doi.org/10.1017/S0263574714000940 Published online by Cambridge University Press

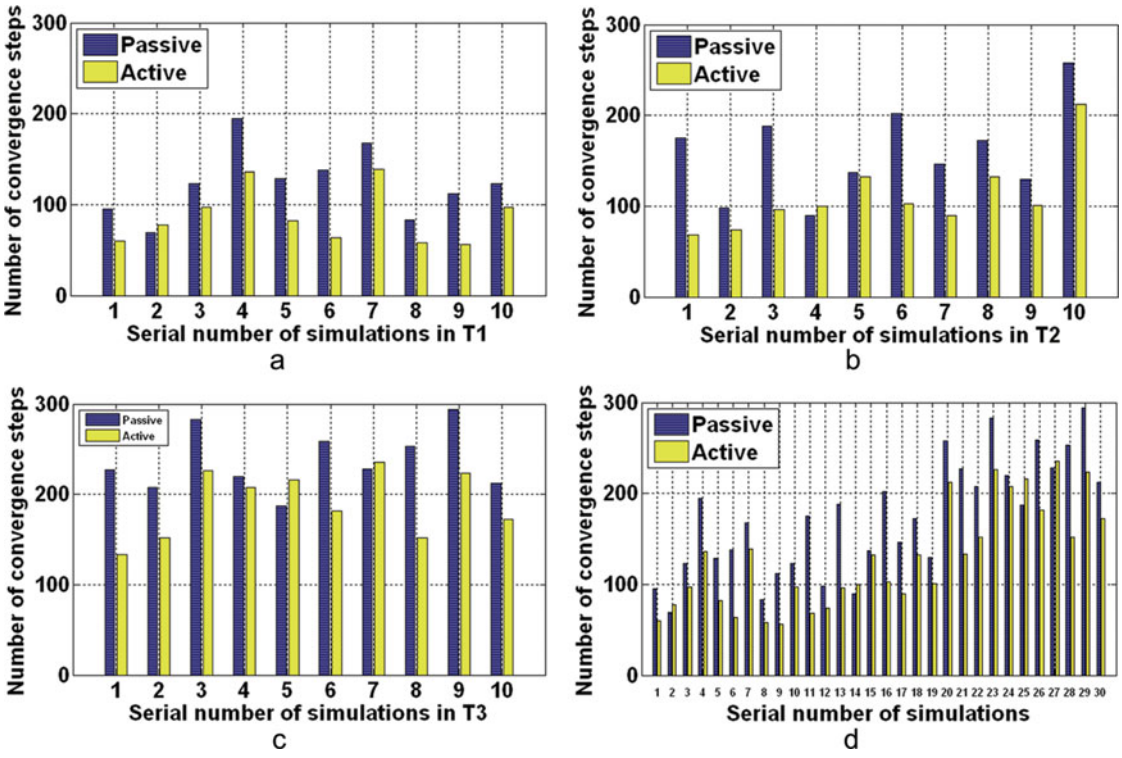


Fig. 10. Comparison of the convergence steps to status A.

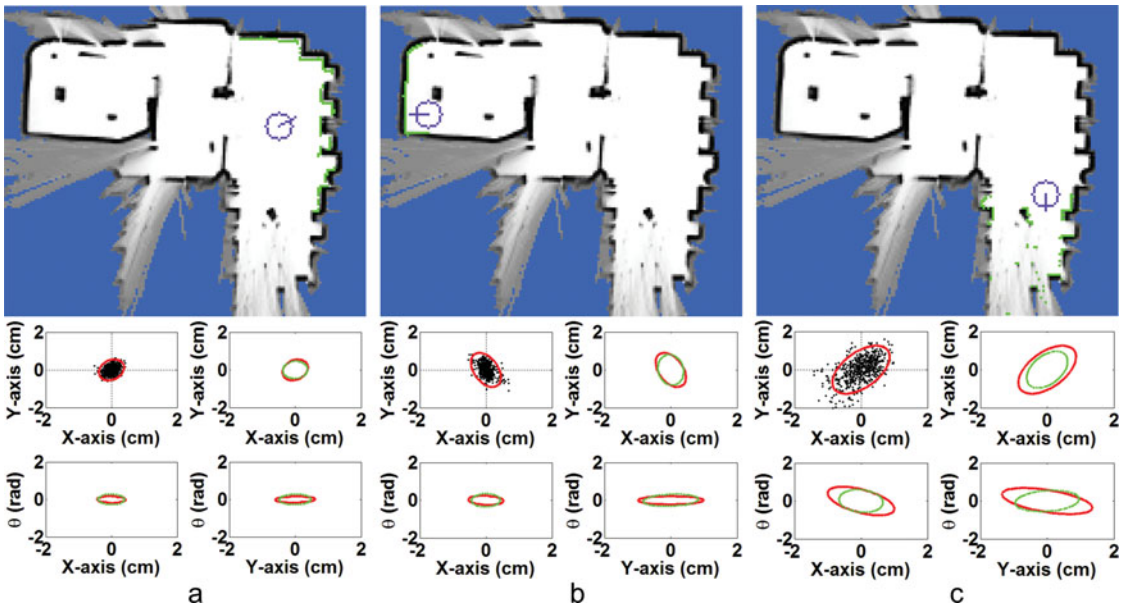


Fig. 11. Precision comparison between covariance ellipses. The upper part of each figure shows the observing environment, and the lower part shows the covariance ellipses of $x-y$, $x-\theta$, and $y-\theta$ respectively.

which brings more noises to both the prior-map (during mapping process) and observations. In the localizability matrix, the unhelpful information, such as the map noises and bias term of observations, has been taken into account definitely. That means the evaluation of observations in the localizability matrix is reasonable. Thus, although the two covariance ellipses have deviation, their fundamental shape is still consistent. Please note, estimating the covariance through the classical PF needs several filtering steps and a large amount of particles, which cannot be used in real-time. But through the

https://doi.org/10.1017/S0263574714000940 Published online by Cambridge University Press

localizability matrix, the covariance can be calculated directly and numerically. From the above analysis, the localizability matrix is verified to be able to evaluate the observations in environments with different degrees of uncertainty. Naturally, the validation of localizability, i.e. the determinant of the localizability matrix, is achieved.

4.3.2. Global localization in a real environment. The comparative experiments are demonstrated in a real environment. For each comparison, the initial conditions, such as the initial actual robot pose, the initial particle distribution, are the same for the passive and the proposed active global localization algorithms.

Figure 12 shows one experiment of the proposed active algorithm. In screenshots, the red circle is defined as the robot pose estimated by all the particles, and the green circle is the robot pose estimated by the particles with high importance weight $w_t^{(k)} \geq 0.7$. The robot found its actual pose in about Step 54.

Figure 13(a) shows the matching weight curves of the passive and the proposed active algorithms. When there are no particles with the high importance weight, the matching weight is the average importance weight of all the particles; or it is the average importance weight of the particles with $w_t^{(k)} \geq 0.7$. The matching weight curve of the proposed algorithm becomes stable more quickly (in about Step 42 of the proposed active algorithm, and in about Step 79 of the passive algorithm). Figure 13(b) shows the convergence curves of particles. The results are similar, as can be seen in Fig. 13(a), thus the convergence of particles is more efficient based on the proposed active algorithm (the proposed active algorithm converged in about Step 50, while the passive algorithm converged in about Step 82). The comparative experiments with the different initial conditions were done a total of 10 times. The statistical results were nearly the same as the simulations, which demonstrates the effectiveness (efficiency and robustness) of the proposed algorithm.

In experiments, for convenience, the matching weight is used to reflect the localization accuracy instead of measuring the deviation between the actual and the estimated robot poses. When the algorithm converged, the average deviation of the final position is about 0.14 m, and the average deviation of the final heading is about 2.69°.

4.3.3. Comparison of experimental results among active algorithms. Compared to the passive algorithm, the active algorithms including the proposed one can enhance the robustness against the system ambiguities. Since it is difficult to compare the robustness among these different active algorithms, the execution time is compared and analyzed here. In experiments, the execution time of one step (including the action selection and particle filtering) of the proposed algorithm is 2.80 s on average, when using 3000 particles (most time is consumed in evaluating the importance weights of particles). In the environment, whose area is 75×80 m^2, the total time of active global localization is 240 s on average (the mobile robot is in scenario T1 initially).

For the active global localization algorithms in refs. [25] and [26], although the computational complexity of selecting one action is not great (see Section 3.3), much more time will be wasted in extraction of the observation features, as the geometric prior-map is used in these algorithms. The authors in ref. [26] did not give the exact execution time, but if the proposed action selection mechanism is introduced into the pre-convergence process of ref. [26], its execution time would be further reduced. The execution time of one step in ref. [25] is given through simulations. A run of the active strategy needs about 87 s (Intel Core2 Duo 1.86GHz CPU, 2G RAM); and to finish the whole global localization in a 100×100 m^2 environment, several steps are needed. The execution time of the proposed algorithm is much smaller than that in ref. [25]. Additionally, as the above algorithms used the geometric prior-map, they cannot deal with the unspecific structures or noises of the prior-map and there will be some limitation for the real application.

For the entropy-based active global localization algorithm in ref. [22], the total time of finishing the active global localization in a 23×4.5 m^2 environment is about 600 s (Intel Pentium-200 CPU). In ref. [24], the authors used 150 particles to reduce the cost of approximating the entropy; and then the execution time is about 0.2 s (Intel Pentium-4 1.8GHz CPU). But in the larger environment, the execution time is still large while the particles increase, as the computational complexity is related to the square of the particle number. The above comparisons indicate the higher efficiency of the proposed algorithm for the following reasons: first, the entropy only evaluates the observations without directional information; while the defined localizability can represent both the respective and the

https://doi.org/10.1017/S0263574714000940 Published online by Cambridge University Press

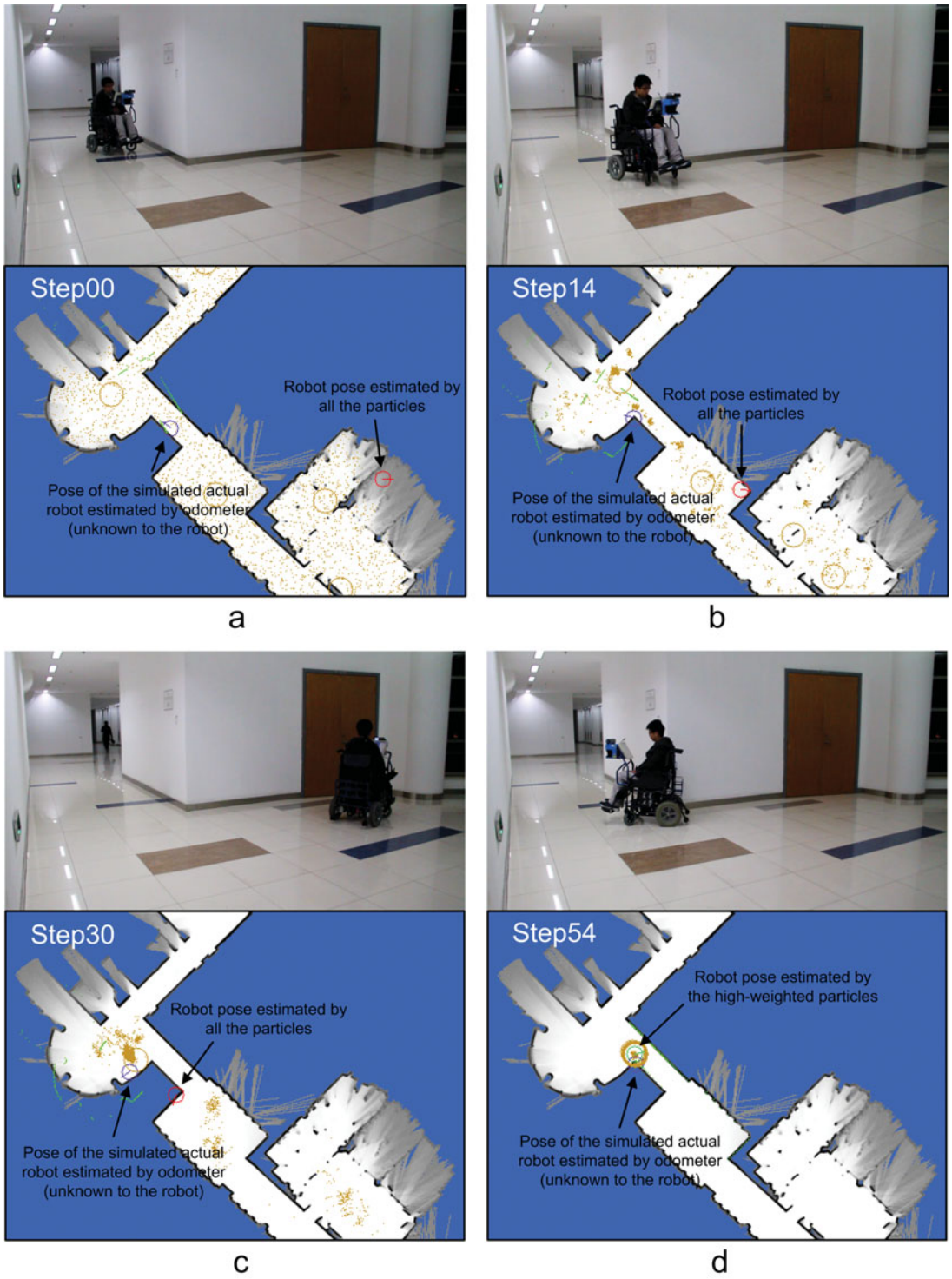


Fig. 12. Active global localization based on the localizability-based action selection mechanism. The upper part of each figure is the real scene and the lower part is the corresponding screenshots of the software interface (partial).

coupling influences on localization among x, y, and θ states, which is suitable to evaluate observations in environments with different degrees of uncertainty. Second, the entropy-based algorithm controlled the robot to the place where the observation uncertainty is smaller; while the proposed algorithm guided the robot to the place where the distinctness of the observation uncertainty before and after the action is maximum. Finally, in the entropy-based algorithm, the robot is driven according to the state

https://doi.org/10.1017/S0263574714000940 Published online by Cambridge University Press

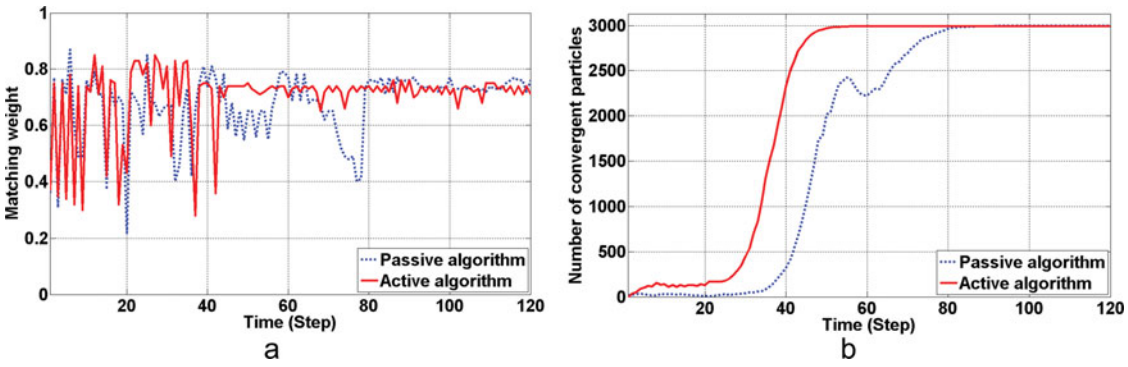


Fig. 13. Comparison of the matching weight and particle convergence.

space information; while in the proposed algorithm, the robot is driven according to the observation distinctness. In summary, that is why the proposed algorithm has less computational load.

5. Conclusion

In this study, an active global localization based on the localizability-based action selection mechanism is proposed. The most noticeable difference is that, taking the uncertainty of the prior-map into account, the mobile robot is guided to achieve the effective observations of the whole particle system through maximization of the localizability distinctness. As a result, it accelerates the convergence and enhances the robustness of global localization. The algorithm does not extract any specific features from the observations; and compared with the passive algorithm, the computational complexity of the proposed active algorithm does not increase significantly as the localizability is pre-cached off-line.

In simulations, global localization using the passive and the proposed active algorithms are compared in the environments with different degrees of uncertainty. The results show that fewer steps are needed to localize the robot when using the proposed active algorithm. There are also fewer failures in different scenarios, which indicates the enhanced robustness against the system ambiguities. In experiments, through the comparison of the covariance ellipses estimated by the scan-matching algorithm and the localizability matrix, the ability of the proposed localizability (i.e. the determinant of the localizability matrix) to evaluate the observations reasonably and properly is verified. Additionally, the comparative experiments between the passive and the proposed active algorithms are implemented in a real environment based on an intelligent wheelchair platform. The experimental results also demonstrate the effectiveness (efficiency and robustness) of the proposed algorithm as simulations. Finally, through comparison of the experimental results among the existing active global localization algorithms, the lower computational load of the proposed algorithm is verified.

As a future enhancement, the real timing of the proposed algorithm could be improved further through introducing the KLD (Kullback-Leibler distance)-sampling or pre-caching more information. Then we will implement the localizability in a multi-robot global localization to achieve a faster convergence and stronger robustness of the algorithm.

This study is partly supported by National High Technology Research and Development Program of China (2012AA041403), Natural Science Foundation of China (60934006, 61175088), Research Fund for the Doctoral Program of Higher Education (20100073110018), and State Key Laboratory of Robotics and System (HIT) (SKLRS2011ZD01).

References

1. J. Borenstein, B. Everett and L. Feng, *Navigating Mobile Robots: Systems and Techniques* (A. K. Peters, Ltd., Wellesley, MA, 1996).
2. G. Weiss, C. Wetzler and E. V. Puttkamer, "Keeping Track of Position and Orientation of Moving Indoor Systems by Correlation of Range-Finder Scans," *Proceedings of the IEEE/RSJ International Conference on Intelligent Robots and Systems (IROS)*, Munich, Germany (September 12–16, 1994) pp. 595–601.

https://doi.org/10.1017/S0263574714000940 Published online by Cambridge University Press

3. Y. Wang and W. D. Chen, "Hybrid Map-Based Navigation for Intelligent Wheelchair," *Proceedings of the IEEE International Conference on Robotics and Automation (ICRA)*, Shanghai, China (May 9–13, 2011) pp. 637–642.
4. S. Thrun, W. Burgard and D. Fox, *Probabilistic Robotics* (MIT Press, Cambridge, MA, 2005).
5. W. Burgard, D. Fox, D. Hennig and T. Schmidt, "Estimating the Absolute Position of a Mobile Robot Using Position Probability Grids," *Proceedings of the National Conference on Artificial Intelligence (AAAI)*, Portland, USA (August 4–8, 1996) pp. 896–901.
6. P. Jensfelt and S. Kristensen, "Active global localisation for a mobile robot using multiple hypothesis tracking," *IEEE Tran. Robot. Autom.* **17**(5), 748–760 (2001).
7. S. Thrun, D. Fox, W. Burgard and F. Dellaert, "Robust Monte Carlo localization for mobile robots," *Artif. Intell.* **128**(1–2), 99–141 (2001).
8. E. Menegatti, M. Zoccarato, E. Pagello and H. Ishiguro, "Image-based Monte Carlo localisation with omnidirectional images," *Robot. Auton. Syst.* **47**(4), 251–267 (2004).
9. H. H. Lin and C. C. Tsai, "Improved global localization of an indoor mobile robot via fuzzy extended information filtering," *Robotica* **26**, 241–254 (2008).
10. M. Rao, G. Dudek and S. Whitesides, "Randomized algorithms for minimum distance localization," *Int. J. Robot. Res.* **26**, 917–933 (2007).
11. J. M. O'Kane, "Global Localization Using Odometry," *Proceedings of the IEEE International Conference on Robotics and Automation (ICRA)*, Orlando, USA (May 15–19, 2006) pp. 37–42.
12. T. He and S. Hirose, "A global localization approach based on line-segment relationmatching technique," *Robot. Auton. Syst.* **60**(1), 95–112 (2012).
13. L. Zhang, R. Zapata and P. Lépinay, "Self-adaptive Monte Carlo localization for mobile robots using range finders," *Robotica* **30**, 229–244 (2012).
14. G. H. Cen, N. Matsuhira, J. Hirokawa, H. Ogawa and I. Hagiwara. "Mobile Robot Global Localization Using Particle Filters," *Proceedings of the IEEE International Conference on Control, Automation and Systems (ICCAS)*, Seoul, Korea (October 14–17, 2008) pp. 710–713.
15. C. Tovey and S. Koenig, "Localization: Approximation and performance bounds to minimize travel distance," *IEEE Tran. Robot.* **26**(2), 320–330 (2010).
16. K. Hughes and R. R. Murphy, "Ultrasonic Robot Localization Using Dempster-Shafer Theory," *Proceedings of the SPIE Stochastic Methods in Signal Processing, Image Processing, and Computer Vision, Invited Session on Applications for Vision and Robotics, Society of Photo Optical*, San Diego, USA (July 19–23, 1992) pp. 2–11.
17. D. Fox, W. Burgard and S. Thrun, "Markov localization for mobile robots in dynamic environments," *J. Artif. Intell. Res.* **11**, 391–427 (1999).
18. T. Kwo, J. Yang, J. Song and W. Chung, "Efficiency Improvement in Monte Carlo Localization through Topological Information," *Proceedings of the IEEE/RSJ International Conference on Intelligent Robots and Systems (IROS)*, Beijing, China (October 9–15, 2006) pp. 424–429.
19. S. Radacina Rusu, M. J. D. Hayes and J. A. Marshall, "Localization in Large-Scale Underground Environments with RFID," *Proceedings of the IEEE Canadian Conference on Electrical and Computer Engineering (CCECE)*, Niagara Falls, Canada (May 8–11, 2011) pp. 1140–1143.
20. T. He and S. Hirose, "Observation-driven Bayesian filtering for global location estimation in the field area," *J. Field Robot.* **30**, 489–518 (2013).
21. D. Crisan and A. Doucet, "A survey of convergence results on particle filtering methods for practitioners," *IEEE Tran. Signal Process.* **50**(3), 736–746 (2002).
22. D. Fox, W. Burgard and S. Thrun, "Active Markov localization for mobile robots," *Robot. Autom. Syst.* **25**(3–4), 195–207 (1998).
23. A. Doucet, *On Sequential Simulation-Based Methods for Bayesian Filtering* (Technical Report, Signal Processing Group, Department of Engineering, University of Cambridge, 1998).
24. J. M. Porta, J. J. Verbeek and B. J. A. Krose, "Active appearance-based robot localization using stereo vision," *Auton. Robots* **18**(1), 59–80 (2005).
25. A. C. Murtra, J. M. M. Tur and A. Sanfeliu, "Action evaluation for mobile robot global localization in cooperative environments," *Robot. Auton. Syst.* **56**(10), 807–818 (2008).
26. H. J. Zhou and S. Sakane, "Sensor planning for mobile robot localization - A hierarchical approach using a bayesian network and a particle filter," *IEEE Tran. Robot.* **24**(2), 481–487 (2008).
27. J. P. Gonzalez and A. T. Stentz, "Planning with Uncertainty in Position: An Optimal and Efficient Planner," *Proceedings of the IEEE/RSJ International Conference on Intelligent Robots and Systems (IROS)*, Edmonton, Canada (August 2–6, 2005) pp. 2435–2442.
28. A. Censi, "An Accurate Closed-Form Estimate of ICP's Covariance," *Proceedings of the IEEE International Conference on Robotics and Automation (ICRA)*, Roma, Italy (April 10–14, 2007) pp. 3167–3172.
29. A. Censi, D. Calisi, A. de Luca and G. Oriolo, "A Bayesian Framework for Optimal Motion Planning with Uncertainty," *Proceedings of the IEEE International Conference on Robotics and Automation (ICRA)*, Pasadena, USA (May 19–23, 2008) pp. 1798–1805.
30. A. Censi, A. Franchi, L. Marchionni and G. Oriolo, "Simultaneous calibration of odometry and sensor parameters for mobile robots," *IEEE Tran. Robot.* (2013) to appear.
31. Y. Wang, W. D. Chen, J. C. Wang and W. Wang, "Improved particle filter localization in crowed environments for mobile robots," *Robotica* **34**(5), 596–603 (2012).

https://doi.org/10.1017/S0263574714000940 Published online by Cambridge University Press

32. Z. Liu, W. D. Chen, Y. Wang and J. C. Wang, "Localizability Estimation for Mobile Robots Based on Probabilistic Grid Map and its Applications to Localization," *Proceedings of the IEEE International Conference on Multisensor Fusion and Information Integration (MFI)*, Hamburg, Germany (September 13–15, 2012) pp. 46–51.
33. Y. Wang, W. D. Chen, J. C. Wang and H. S. Wang, "Action Selection Based on Localizability for Active Global Localization of Mobile Robots," *Proceedings of the IEEE International Conference on Mechatronics and Automation (ICMA)*, Chengdu, China (August 5–8, 2012) pp. 2071–2076.
34. Y. Bar-Shalom, *Tracking and Data Association* (Academic Press Professional, San Diego, USA, 1987).
35. R. Simmons, D. Goldberg, A. Goode, M. Montemerlo, N. Roy, A. C. Schultz, M. Abramson, I. Horswill, D. Kortenkamp and B. Maxwell, "Grace: An autonomous robot for the AAAI robot challenge," *AI Magazine* **24**(2), 51–72 (2003).
36. B. Z. Bobrovsky and M. Zakai, "A lower bound on the estimation error for markov processes," *IEEE Tran. Autom. Control* **20**(6), 785–788 (1975).
37. A. Censi, "On Achievable Accuracy for Range-Finder Localization," *Proceedings of the IEEE International Conference on Robotics and Automation (ICRA)*, Roma, Italy (April 10–14, 2007) pp. 4170–4175.
38. Y. Bar-Shalom, X. R. Li and T. Kirubarajan, *Estimation with Applications to Tracking and Navigation* (John Wiley & Sons, Inc., New York, 2001).
39. R. M. Gray and D. L. Neuhoff, "A history of k-means type of algorithms," *IEEE Tran. Inf. Theory* **44**, 2325–2384 (1998).
40. G. Antonelli, S. Chiaverini and G. Fusco, "A calibration method for odometry of mobile robots based on the least-squares technique: Theory and experimental validation," *IEEE Tran. Robot.* **21**(5), 994–1004 (2005).
41. M. Montemerlo, N. Roy and S. Thrun, "Perspectives on Standardization in Mobile Robot Programming: The Carnegie Mellon Navigation (CARMEN) Toolkit," *Proceedings of the IEEE/RSJ International Conference on Intelligent Robots and Systems (IROS)*, Las Vegas, USA (October 27–31, 2003) pp. 2436–2441.
42. R. De Maesschalck, D. Jouan-Rimbaud and D. L. Massart, "The Mahalanobis distance," *Chemometr. Intell. Lab. Syst.* **50**(1), 1–18 (2000).

https://doi.org/10.1017/S0263574714000940 Published online by Cambridge University Press